Journal of Astronomical Telescopes, Instruments, and Systems

AstronomicalTelescopes.SPIEDigitalLibrary.org

Computation of misalignment and primary mirror astigmatism figure error of two-mirror telescopes

Zhiyuan Gu
Yang Wang
Guohao Ju
Changxiang Yan

SPIE.

Zhiyuan Gu, Yang Wang, Guohao Ju, Changxiang Yan, "Computation of misalignment and primary mirror astigmatism figure error of two-mirror telescopes," *J. Astron. Telesc. Instrum. Syst.* **4**(1), 019002 (2018), doi: 10.1117/1.JATIS.4.1.019002.

Computation of misalignment and primary mirror astigmatism figure error of two-mirror telescopes

Zhiyuan Gu,[a,*] Yang Wang,[b] Guohao Ju,[a] and Changxiang Yan[a]
[a]Chinese Academy of Science, Changchun Institute of Optics, Fine Mechanics and Physics, Changchun, China
[b]Changchun University of Science and Technology, School of OptoElectronic Engineering, Changchun, China

Abstract. Active optics usually uses the computation models based on numerical methods to correct misalignments and figure errors at present. These methods can hardly lead to any insight into the aberration field dependencies that arise in the presence of the misalignments. An analytical alignment model based on third-order nodal aberration theory is presented for this problem, which can be utilized to compute the primary mirror astigmatic figure error and misalignments for two-mirror telescopes. Alignment simulations are conducted for an R-C telescope based on this analytical alignment model. It is shown that in the absence of wavefront measurement errors, wavefront measurements at only two field points are enough, and the correction process can be completed with only one alignment action. In the presence of wavefront measurement errors, increasing the number of field points for wavefront measurements can enhance the robustness of the alignment model. Monte Carlo simulation shows that, when -2 mm $\leq$ linear misalignment ≤ 2 mm, -0.1 deg $\leq$ angular misalignment ≤ 0.1 deg, and $-0.2\lambda \leq$ astigmatism figure error (expressed as fringe Zernike coefficients C_5/C_6, $\lambda = 632.8$ nm) $\leq 0.2\lambda$, the misaligned systems can be corrected to be close to nominal state without wavefront testing error. In addition, the root mean square deviation of RMS wavefront error of all the misaligned samples after being corrected is linearly related to wavefront testing error. [DOI: 10.1117/1.JATIS.4.1.019002]

Keywords: active optics; alignment; misalignments; astigmatic figure error; nodal aberration theory; two-mirror telescope.

Paper 17076 received Sep. 21, 2017; accepted for publication Feb. 5, 2018; published online Feb. 28, 2018.

1 Introduction

Two-mirror telescopes have an important application in astronomy and other science. Modern two-mirror telescopes commonly used are generally divided into two categories: aplanatic telescopes (e.g., R–C telescopes) and nonaplanatic telescopes (e.g., Cassegrain and Gregorian telescopes). In Cassegrain and Gregorian telescopes, the primary mirror (PM) and secondary mirror (SM) correct spherical aberration independently. The field of view is mainly limited by coma with a linear field dependence. The R–C telescope can correct the third-order spherical aberration and coma simultaneously, so the imaging field can be larger than that of the nonaplanatic telescope, and its imaging field is mainly limited by the third-order astigmatism with a quadratic field dependence.

The aperture of a modern two-mirror telescope is growing larger and larger. With the influence of gravity, temperature, and other factors, misalignments and figure error always occur in telescopes. An active optics system is installed for real-time correction, which can correct errors arising from incorrect optical manufacturing, deformations, and misalignments due to gravity or thermal reasons.

The active optics correction can be divided into rigid-body alignment error correction and figure error correction. For two-mirror telescopes, SM is less affected by stress and temperature gradient because of its smaller aperture. We usually do not correct its figure error, and only rigid-body alignment error correction is needed. While the aperture of PM is usually relatively large, figure error is more likely to occur, and astigmatism is the most common figure error. This paper focuses on computation of misalignment and PM astigmatism figure error parameters of two-mirror telescopes.

For the alignment of two-mirror telescopes, McLeod[1] proposed an alignment method for fast wide-field two-mirror telescopes, which first correct coma and then correct the astigmatism. He deduced the analytic relationship between the ellipticity and position angles of slightly defocused images and the misalignments. The calculation of the misalignments is achieved by measuring the image shape of the off-axis field of view. Noethe and Guisard[2] derived formulas for all parameters defining the field astigmatism of misaligned two-mirror telescopes with arbitrary geometries and stop positions anywhere on the line connecting the vertices of the two mirrors. They applied their formulas to alignment of the ESO Very Large Telescope. Holzlöhner et al.[3] used fifth-order aberration theory to deduce misalignments and optical surface deformations of a telescope from its star images.

There are also some numerical models for optical system alignment, such as the sensitivity matrix model,[4,5] differential wavefront sampling method,[6,7] and merit function regression method.[8] At present, the sensitivity matrix model is used as the most common active optics correction algorithm, and it has been used in many astronomical telescope projects.[4,5] The model represents the Zernike coefficients that characterize the wavefront error of a misaligned system as a linear combination of misalignments. A linear system of equations is established for the Zernike coefficient and misalignments, which can be used to solve misalignments. There is a problem with this method: it cannot bring high accuracy to the estimation of

*Address all correspondence to: Zhiyuan Gu, E-mail: zhiyuan.gu@hotmail.com

2329-4124/2018/$25.00 © 2018 SPIE

the misalignment parameters if the misalignment values are large, as a result of the nonlinearity of the Zernike coefficient sensitivity to the alignment parameters.[8–10] In addition, it is based on data reduction and numerical methods but without a tie to aberration theory.

The nodal aberration theory (NAT) is to study the aberration theory of an optical system with decentered and tilted components. Its initial idea was raised by Shack,[11,12] and later Thompson further developed the theory.[13–18] Schmid et al.[19] used NAT to study the alignment for two-mirror telescopes, and developed some important rules. He first explained why the assumption that perfect performance on axis ensures a fully aligned telescope is false based on NAT. He also analyzed the aberration field of the misaligned two-mirror system with the astigmatism error of the PM (pupil), and found that the location denoting the midpoint of the two astigmatic nodes does not vary with figure errors (at a pupil), and it is solely dependent on misalignments.[20] The key insight to accomplish this distinction is to recognize that after aligning the telescope for zero field-constant coma, one astigmatic node remains effectively at the field center when there is no astigmatic figure error. Consequently, astigmatism measured at the center of the field directly reveals the existence of an astigmatic figure component on the PM. However, there is no more in-depth discussion for quantitative calculation method of misalignments in the above research.

In the research described below, we propose a method based on NAT for calculating the misalignments and PM astigmatism figure error of two-mirror telescopes on the basis of Schmid's work. Section 2 briefly introduces the NAT and details the establishment of the computation model for a misaligned two-mirror telescope. In Sec. 3, an R–C telescope is used to carry out alignment simulation experiments, which include the alignment experiment with and without wavefront testing error, and the Monte Carlo alignment experiment. Section 4 summarizes this article.

2 Misalignment-Affected Aberration Fields of Two-Mirror Telescopes

2.1 *Nodal Aberration Theory*

NAT evolved from the aberration theory of rotationally symmetric optical systems. It uses a more general vector form of the wave aberration expansion instead of the scalar form in a rotationally symmetric system, which is expressed as

$$W = \sum_j \sum_p^{\infty} \sum_n^{\infty} \sum_m^{\infty} W_{klm,j}^{(\mathrm{sph,asph})} [\vec{H}_{Aj}^{(\mathrm{sph,asph})} \cdot \vec{H}_{Aj}^{(\mathrm{sph,asph})}]^p \times (\vec{\rho} \cdot \vec{\rho})^n [\vec{H}_{Aj}^{(\mathrm{sph,asph})} \cdot \vec{\rho}]^m \quad k = 2p + m, \qquad l = 2n + m, \tag{1}$$

where the subscript j is the surface number, $W_{klm,j}$ is the wave aberration coefficient for surface j, $\vec{H}_{Aj}$ denotes the effective field height for surface j, and $\vec{\rho}$ is the normalized vector describing the position in the pupil. $\vec{H}_{Aj}$ and $\vec{\rho}$ are shown in Fig. 1. Note that a fundamental concept in NAT is the decomposition of the surface wave aberration contributions into two separate contributions each, one associated with the spherical base curve, the other determined by the aspheric departure (if any) from the spherical base curve. The superscript sph and asph are used to distinguish them.

In Eq. (1), the effective field height vector $\vec{H}_{Aj}^{(\mathrm{sph,asph})}$ (as shown in Fig. 1) is given as

$$\vec{H}_{Aj}^{(\mathrm{sph,asph})} = \vec{H} - \vec{\sigma}_j^{(\mathrm{sph,asph})}. \tag{2}$$

The vector $\vec{\sigma}_j^{(\mathrm{sph,asph})}$ was first introduced by Buchroeder,[21] which represents the decentration of the center of the aberration field of surface with respect to the optical axis ray (OAR) intercept with the Gaussian image plane. OAR is the ray that is emitted from the center of the field of view and passes through the center of the aperture stop. In a rotationally symmetric system, the OAR coincides with the z-axis (optical axis), as shown in Fig. 2. $\vec{\sigma}_j^{(\mathrm{sph,asph})}$ is called aberration field decenter vectors in NAT, which depends on the misalignments of optical elements.

For the spherical surface contribution to the aberration field, as detailed by Thompson,[14,15] the location of the center of symmetry for the surface contribution is given by

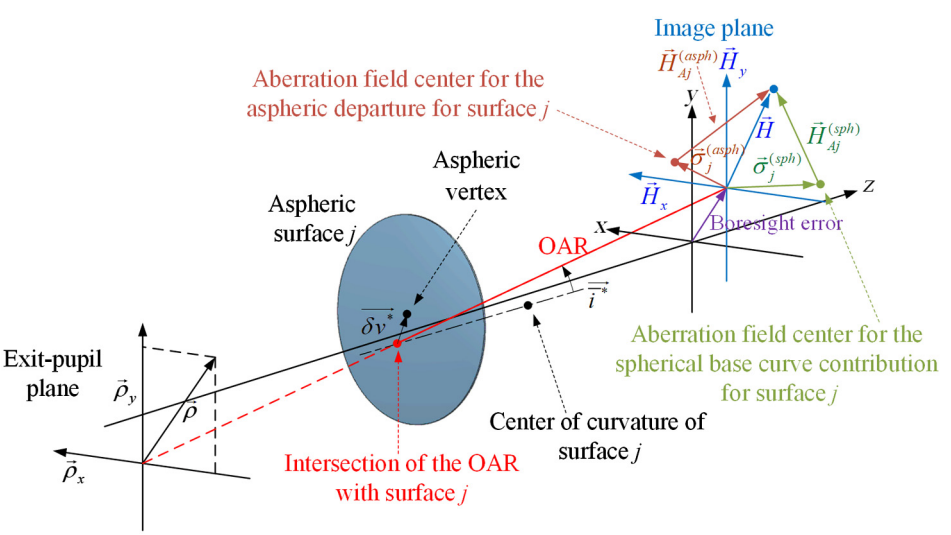

Fig. 1 Concepts of effective field height and aberration field decenter vectors.

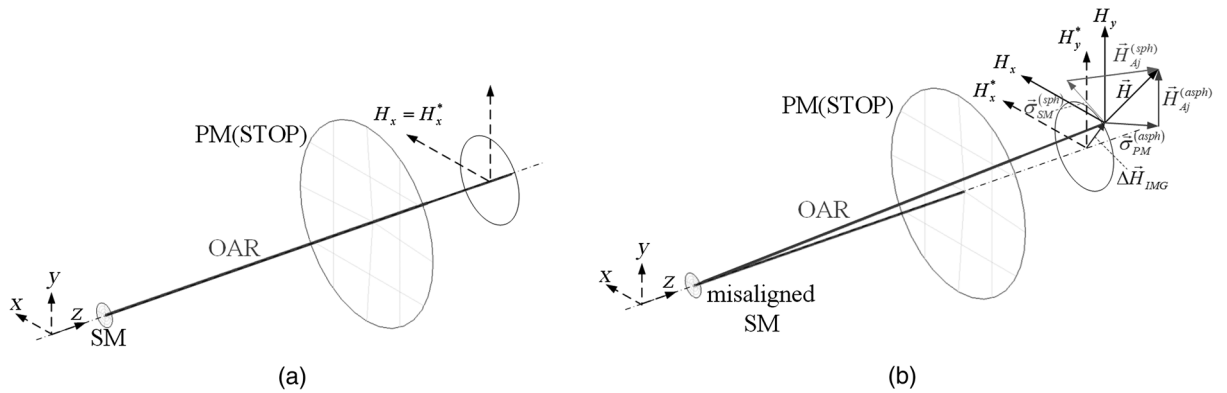

Fig. 2 (a) OAR for an aligned two-mirror telescope with the stop on the PM. Note that OAR coincides with optical axis in an aligned two-mirror telescope (b) OAR in the presence of SM misalignments, which no longer coincides with the optical axis. Concepts of effective field height, aberration field decenter vectors, and boresight error ($\Delta\vec{H}_{\text{IMG}}$) are also shown.

$$\vec{\sigma}_j^{(\text{sph})} = -\frac{\overrightarrow{\overline{u}^{\#}_{\text{OAR}\,j}} - \overrightarrow{\beta^{\#}_{0\,j}} + \overrightarrow{\overline{y}^{\#}_{\text{OAR}\,j}} \cdot c_j}{\overline{u}_j + \overline{y}_j c_j}, \tag{3}$$

where $\overrightarrow{\overline{u}^{\#}_{\text{OAR}\,j}}$ denotes the OAR paraxial angle prior to surface j referenced to the z-axis. $\overrightarrow{\overline{y}^{\#}_{\text{OAR}\,j}}$ denotes the OAR intersection height at surface j referenced to the z-axis. c_j denotes the curvature of surface j. $\overline{u}_j$ corresponds to the paraxial chief ray angle incident at surface j. $\overline{y}_j$ corresponds to the paraxial chief ray height at surface j, and $\overrightarrow{\beta^{\#}_{0\,j}}$ corresponds to the equivalent tilt of surface j,[15] which is related to the misalignments. $\overrightarrow{\beta^{\#}_{0\,j}}$ is given by

$$\overrightarrow{\beta^{\#}_{0\,j}} = \begin{bmatrix} -\text{BDE}_j + \text{XDE}_j c_j \\ \text{ADE}_j + \text{YDE}_j c_j \end{bmatrix}. \tag{4}$$

A right-handed coordinate system is utilized in our paper. In a misaligned or generally nonsymmetric optical system, there are six kinds of misalignments, which are the decenter along the x-, y-, and z-axes (XDE, YDE, and ZDE) and the tilts in $y-z$ plane, x–z plane, and x–y plane (ADE, BDE, and CDE), respectively (referred to as DAR, decenter and return in CODE V). A positive XDE/YDE is the displacement in the $+x/y$ direction, and a positive ADE/BDE is the rotation which is left handed about the $+x/y$ axis.

The location of the aspheric contribution is located at[14,15]

$$\vec{\sigma}_j^{(\text{asph})} = \frac{\overrightarrow{\delta v_j^*}}{\overline{y}_j} = \frac{1}{\overline{y}_j}\left(\begin{bmatrix} \text{XDE}_j \\ \text{YDE}_j \end{bmatrix} - \overrightarrow{\overline{y}^{\#}_{\text{OAR}\,j}}\right), \tag{5}$$

where $\overrightarrow{\delta v_j^*}$ denotes the intersection height of the OAR with respect to the aspheric vertex of surface j, as shown in Fig. 1.

The mathematical relationship between aberration field decenter vectors and misalignments in the optical systems is given in Eqs. (3) and (5).

2.2 *Aberration Field Decenter Vectors for Individual Surfaces of Two-Mirror Telescopes*

Most large astronomical telescopes in use today have the aperture stop located on the PM. The reason for the particular choice is mainly caused by the large relative cost of the PM aperture size. So in this paper, we focus on the telescopes whose aperture stop locates on the PM. For such telescopes, we can use the PM as the datum for alignment, and use the SM as the misaligned element without losing the generality. The SM actually has a total of six misalignments, which are XDE_{SM}, YDE_{SM}, ZDE_{SM}, ADE_{SM}, BDE_{SM}, and CDE_{SM}. ZDE_{SM} is not studied in the paper because it does not destroy the rotational symmetry of the system, and mainly introduces the spherical aberration and defocus aberration, which can be solved using the axisymmetric aberration theory. Due to the rotational symmetry of the system, the existence of CDE_{SM} does not affect the imaging properties, nor does it introduce any aberration. Therefore, this paper mainly studies the four kinds of misalignments: XDE_{SM}, YDE_{SM}, ADE_{SM}, and BDE_{SM}. The misalignments of SM result in a decentration of the symmetry center of the aberration field. It is necessary to study the relationship between the aberration field decenter vectors and the misalignments to establish the computation model of a misaligned two-mirror system.

The paraxial quantities $\overline{u}_j$ and $\overline{y}_j$ can be derived by traditional paraxial equations for rotationally symmetric optical systems, which are given by

$$\overline{u}_{\text{SM}} = -\overline{u}_{\text{PM}}, \tag{6}$$

$$\overline{y}_{\text{PM}} = 0, \tag{7}$$

$$\overline{y}_{\text{SM}} = -d_1 \overline{u}_{\text{PM}}. \tag{8}$$

The OAR quantities $\overrightarrow{\overline{u}^{\#}_{\text{OAR}\,j}}$ and $\overrightarrow{\overline{y}^{\#}_{\text{OAR}\,j}}$ can be computed by the LCS paraxial ray-trace equations for optical systems with tilted and decentered surfaces as developed by Buchroeder,[21] which are given as

$$\overrightarrow{\overline{u}^{\#}_{\text{OARPM}}} = \overrightarrow{\overline{u}^{\#}_{\text{OARSM}}} = \begin{bmatrix} 0 \\ 0 \end{bmatrix}, \tag{9}$$

$$\overrightarrow{\overline{y}^{\#}_{\text{OARPM}}} = \overrightarrow{\overline{y}^{\#}_{\text{OARSM}}} = \begin{bmatrix} 0 \\ 0 \end{bmatrix}. \tag{10}$$

The aberration field decenter vectors for PM and SM can be obtained after substituting Eq. (4), the expressions for the

OAR quantities [Eqs. (9) and (10)] and the paraxial quantities [Eqs. (6)–(8)] into Eqs. (3) and (5), which are given as

$$\vec{\sigma}_{\mathrm{PM}}^{(\mathrm{sph})} = \begin{bmatrix} 0 \\ 0 \end{bmatrix}, \tag{11}$$

$$\vec{\sigma}_{\mathrm{SM}}^{(\mathrm{sph})} = -\frac{1}{u_{pr1}(d_1 + r_{\mathrm{SM}})} \begin{bmatrix} \mathrm{XDE}_{\mathrm{SM}} - \mathrm{BDE}_{\mathrm{SM}} r_{\mathrm{SM}} \\ \mathrm{YDE}_{\mathrm{SM}} + \mathrm{ADE}_{\mathrm{SM}} r_{\mathrm{SM}} \end{bmatrix}, \tag{12}$$

$$\vec{\sigma}_{\mathrm{PM}}^{(\mathrm{asph})} = \begin{bmatrix} 0 \\ 0 \end{bmatrix}, \tag{13}$$

$$\vec{\sigma}_{\mathrm{SM}}^{(\mathrm{asph})} = -\frac{1}{d_1 u_{pr1}} \begin{bmatrix} \mathrm{XDE}_{\mathrm{SM}} \\ \mathrm{YDE}_{\mathrm{SM}} \end{bmatrix}, \tag{14}$$

where r_j denotes the radius of surface j, d_j denotes the thickness of surface j, and $\overline{u}_{\mathrm{PM}}$ is the incident angle of the chief ray at the PM in the nominal system.

The mathematical relationship between aberration field decenter vectors and misalignments in the two-mirror telescopes is given in this section. In the following section, we will derive the mathematical relationship between wavefront aberration and aberration field decenter vectors of two-mirror telescopes. The relationship between coma and astigmatism induced by misalignments and aberration field decenter vectors is derived in Secs. 2.3 and 2.4, respectively. Section 2.5 deduces the contribution of astigmatic figure error of the PM to wave aberrations of two-mirror telescopes. Finally, the equation of wavefront aberration and misalignments can be obtained, and the calculation model of the misalignments is established. The alignment model building process is shown in Fig. 3.

2.3 *Third-Order Coma Aberration Field of Misaligned Two-Mirror Telescopes*

According to third-order NAT, in a misaligned system, coma can be expressed by the following equation:[13]

$$W_{\mathrm{COMA}_3} = [(W_{131}\vec{H} - \vec{A}_{131}) \cdot \vec{\rho}](\vec{\rho} \cdot \vec{\rho}), \tag{15}$$

with $W_{131} = \sum_j W_{131j}$, $\vec{A}_{131} = \sum_j W_{131j}\vec{\sigma}_j$.

For a nonaplanatic telescope (such as R–C telescope), the system corrected third-order coma. The coma aberration field in these telescopes can be expressed as

$$W_{\mathrm{COMA}_3} = [-\vec{A}_{131} \cdot \vec{\rho}](\vec{\rho} \cdot \vec{\rho}). \tag{16}$$

In optical testing, the wavefront at the exit pupil of an optical system is usually fitted into a Zernike polynomial. Therefore, from the practical engineering application point of view, Eq. (16) should be rewritten as a new form that contains the Zernike coefficients. The Seidel coefficients can be expressed exactly as the infinitesimal sum of the Zernike polynomials.[22] However, in the two-mirror system, the high-order Zernike coefficients fitted to the exit pupil plane are very small and can be ignored in the calculation of misalignments. Therefore, it is sufficient to use the first 16 fringe Zernike coefficients to establish the misalignments computation model.

According to the definition of the coordinate system in NAT

$$\vec{\rho} = |\vec{\rho}| \begin{bmatrix} \cos\varphi \\ \sin\varphi \end{bmatrix}, \tag{17}$$

$$\vec{\rho}(\vec{\rho} \cdot \vec{\rho}) = |\vec{\rho}|^3 \begin{bmatrix} \cos\varphi \\ \sin\varphi \end{bmatrix}, \tag{18}$$

leading to

$$W_{\mathrm{COMA}_3} = \begin{bmatrix} W_{131}\vec{H}_x - \vec{A}_{131,x} \\ W_{131}\vec{H}_y - \vec{A}_{131,y} \end{bmatrix} \cdot \begin{bmatrix} |\vec{\rho}|^3 \cos\varphi \\ |\vec{\rho}|^3 \sin\varphi \end{bmatrix},$$

for Cassegrain or Gregorian telescopes, (19)

$$W_{\mathrm{COMA}_3} = \begin{bmatrix} -\vec{A}_{131,x} \\ -\vec{A}_{131,y} \end{bmatrix} \cdot \begin{bmatrix} |\vec{\rho}|^3 \cos\varphi \\ |\vec{\rho}|^3 \sin\varphi \end{bmatrix},$$

for R − C telescopes, (20)

where $\vec{A}_{131,x}$ and $\vec{A}_{131,y}$ are the x- and y-components of $\vec{A}_{131}$, respectively. According to the relationship between the Seidel coefficients and Zernike coefficients

$$\begin{bmatrix} \vec{A}_{131,x} \\ \vec{A}_{131,y} \end{bmatrix} = \begin{bmatrix} W_{131}\vec{H}_x - 3C_{\mathrm{COMA},x} \\ W_{131}\vec{H}_y - 3C_{\mathrm{COMA},y} \end{bmatrix},$$

for Cassegrain or Gregorian telescopes, (21)

$$\begin{bmatrix} \vec{A}_{131,x} \\ \vec{A}_{131,y} \end{bmatrix} = \begin{bmatrix} -3C_{\mathrm{COMA},x} \\ -3C_{\mathrm{COMA},y} \end{bmatrix}, \quad \text{for R} - \text{C telescopes}, \tag{22}$$

with

$$\begin{bmatrix} C_{\mathrm{COMA},x} \\ C_{\mathrm{COMA},y} \end{bmatrix} = \begin{bmatrix} C_7 - C_{10} - 4C_{14} \\ C_8 - C_{11} - 4C_{15} \end{bmatrix}, \tag{23}$$

where C_{COMA} represents the Zernike coma coefficients obtained by wavefront testing, and C_i is the i'th fringe Zernike coefficient.

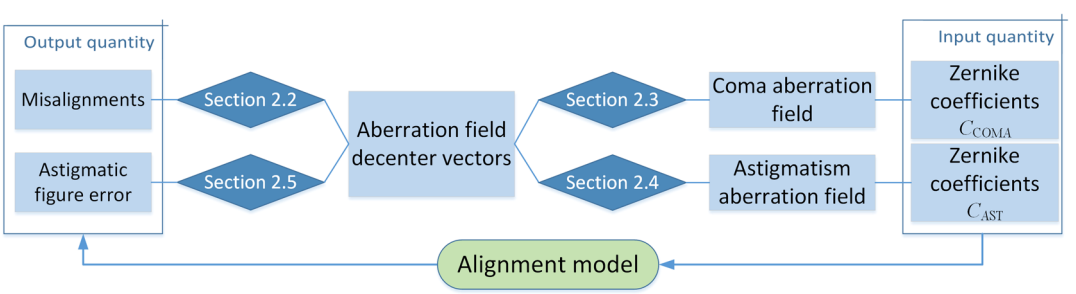

Fig. 3 Alignment model building process.

2.4 *Third-Order Astigmatism Aberration Field of Misaligned Two-Mirror Telescopes*

The third-order astigmatism in the NAT is given by[13]

$$W_{\mathrm{AST}_3} = \frac{1}{2}\left[\sum_j W_{222j}\vec{H}^2 - 2\vec{H}A_{222} + \vec{B}_{222}^2\right]\cdot\vec{\rho}^2, \tag{24}$$

with $W_{222} = \sum_j W_{222j}$, $\vec{A}_{222} = \sum_j W_{222j}\vec{\sigma}_j$, and $\vec{B}_{222}^2 = \sum_j W_{222j}\vec{\sigma}_j^2$.

From the Eq. (24), we can see that misalignments additionally introduce the field-linear astigmatism and field-constant astigmatism.

According to the definition of the coordinate system in NAT

$$\vec{\rho}^2 = \rho^2\begin{bmatrix}\cos 2\varphi\\ \sin 2\varphi\end{bmatrix}, \tag{25}$$

leading to

$$W_{\mathrm{AST}_3} = \begin{bmatrix}\frac{W_{222}(\vec{H}_x^2-\vec{H}_y^2)}{2} - \vec{H}_x\vec{A}_{222,x} + \vec{H}_y\vec{A}_{222,y} + \frac{\vec{B}_{222,x}^2}{2}\\ W_{222}\vec{H}_x\vec{H}_y - \vec{H}_x\vec{A}_{222,y} - \vec{H}_y\vec{A}_{222,x} + \frac{\vec{B}_{222,y}^2}{2}\end{bmatrix} \cdot \begin{bmatrix}|\vec{\rho}|^2\cos(2\varphi)\\ |\vec{\rho}|^2\sin(2\varphi)\end{bmatrix}. \tag{26}$$

According to the relationship between the Seidel coefficients and Zernike coefficients

$$\begin{bmatrix}-\vec{H}_x & \vec{H}_y & \frac{1}{2} & 0\\ -\vec{H}_y & -\vec{H}_x & 0 & \frac{1}{2}\end{bmatrix}\begin{bmatrix}\vec{A}_{222,x}\\ \vec{A}_{222,y}\\ \vec{B}_{222,x}^2\\ \vec{B}_{222,y}^2\end{bmatrix} = \begin{bmatrix}C_{\mathrm{AST},x} - \frac{W_{222}}{2}(\vec{H}_x^2 - \vec{H}_y^2)\\ C_{\mathrm{AST},y} - W_{222}\vec{H}_x\vec{H}_y\end{bmatrix}, \tag{27}$$

with

$$\begin{bmatrix}C_{\mathrm{AST},x}\\ C_{\mathrm{AST},y}\end{bmatrix} = \begin{bmatrix}C_5 - 3C_{12}\\ C_6 - 3C_{13}\end{bmatrix}, \tag{28}$$

where C_{AST} represents the Zernike astigmatism coefficients obtained by wavefront testing.

2.5 *Astigmatic Aberration Field Introduced by Astigmatic Figure Error of the PM*

The astigmatism figure error can be easily expressed with the Zernike polynomial (fringe Zernike polynomial Z_5 and Z_6 terms). Zernike astigmatism needs to be introduced into the NAT computation model, which can be expressed as follows:

$$\begin{bmatrix}{}_{(\mathrm{FIGURE})}C_5\\ {}_{(\mathrm{FIGURE})}C_6\end{bmatrix}\cdot\begin{bmatrix}Z_5\\ Z_6\end{bmatrix} = \begin{bmatrix}{}_{(\mathrm{FIGURE})}C_5\\ {}_{(\mathrm{FIGURE})}C_6\end{bmatrix}\cdot\begin{bmatrix}|\vec{\rho}|^2\cos 2\varphi\\ |\vec{\rho}|^2\sin 2\varphi\end{bmatrix}, \tag{29}$$

where ${}_{(\mathrm{FIGURE})}C_5$ and ${}_{(\mathrm{FIGURE})}C_6$ are astigmatic figure errors of the PM expressed by the Fringe Zernike astigmatic coefficients C_5 (axis at 0 deg or 90 deg) and C_6 (axis at ± 45 deg), respectively.

When the PM with the astigmatism figure error is the stop surface, the imaging beams of the different field of view have the same footprint on the PM. At the same time, since the field of view of the two-mirror telescope is very small, it can be considered that the effect of the astigmatism error is the same for the imaging beam of different fields. Therefore, it can be concluded that when the PM is the aperture stop, the astigmatism figure error on the PM is introduced into field-constant astigmatism. Based on this argument, it is only necessary to add the field-constant astigmatism introduced by figure error into the field-constant astigmatism introduced by misalignments, and the wave aberration expression of the two-mirror telescope that has astigmatic figure error on PM can be obtained.

The field-constant astigmatism ${}_{(\mathrm{FIGURE})}\vec{B}_{222}^2$ introduced by figure error is added to the field-constant astigmatism ${}_{(\mathrm{MISALIGN})}\vec{B}_{222}^2$ introduced by misalignments, given as

$$\begin{aligned}\vec{B}_{222}^2 &= {}_{(\mathrm{MISALIGN})}\vec{B}_{222}^2 + {}_{(\mathrm{FIGURE})}\vec{B}_{222}^2\\ &= \sum_j W_{222j}\vec{\sigma}_j^2 + {}_{(\mathrm{FIGURE})}\vec{B}_{222}^2,\end{aligned} \tag{30}$$

so the wave aberration introduced by the figure error is given by

$$\begin{aligned}{}_{(\mathrm{FIGURE})}W_{\mathrm{ATS3}} &= \frac{1}{2}{}_{(\mathrm{FIGURE})}\vec{B}_{222}^2\cdot\vec{\rho}^2\\ &= \frac{1}{2}{}_{(\mathrm{FIGURE})}\vec{B}_{222}^2\begin{bmatrix}|\vec{\rho}|^2\cos 2\varphi\\ |\vec{\rho}|^2\sin 2\varphi\end{bmatrix}.\end{aligned} \tag{31}$$

According to the relationship between optical path difference and figure error, the wave aberration introduced by the figure error also can be expressed by

$${}_{(\mathrm{FIGURE})}W_{\mathrm{ATS3}} = (n'-n)\begin{bmatrix}{}_{(\mathrm{FIGURE})}C_5\\ {}_{(\mathrm{FIGURE})}C_6\end{bmatrix}\cdot\begin{bmatrix}|\vec{\rho}|^2\cos 2\varphi\\ |\vec{\rho}|^2\sin 2\varphi\end{bmatrix}, \tag{32}$$

leading to

$${}_{(\mathrm{FIGURE})}\vec{B}_{222}^2 = -4\begin{bmatrix}{}_{(\mathrm{FIGURE})}C_5\\ {}_{(\mathrm{FIGURE})}C_6\end{bmatrix}. \tag{33}$$

Therefore, when the PM has an astigmatism error, Eq. (27) should be rewritten as

$$\begin{aligned}&\begin{bmatrix}-\vec{H}_x & \vec{H}_y & \frac{1}{2} & 0\\ -\vec{H}_y & -\vec{H}_x & 0 & \frac{1}{2}\end{bmatrix}\begin{bmatrix}\vec{A}_{222,x}\\ \vec{A}_{222,y}\\ {}_{(\mathrm{MISALIGN})}\vec{B}_{222,x}^2\\ {}_{(\mathrm{MISALIGN})}\vec{B}_{222,y}^2\end{bmatrix}\\ &= \begin{bmatrix}C_{\mathrm{AST},x} + 2{}_{(\mathrm{FIGURE})}C_5 - \frac{W_{222}(\vec{H}_x^2-\vec{H}_y^2)}{2}\\ C_{\mathrm{AST},y} + 2{}_{(\mathrm{FIGURE})}C_6 - \vec{H}_x\vec{H}_y W_{222}\end{bmatrix}.\end{aligned} \tag{34}$$

Utilizing Eqs. (11)–(14), (21), (22), and (34), we can establish a computation model of misalignment and PM astigmatism figure error parameters of two-mirror telescopes. Four equations can be established with wavefront testing of a field point. A total of six parameters are to be solved, which are $\mathrm{XDE}_{\mathrm{SM}}$, $\mathrm{YDE}_{\mathrm{SM}}$, $\mathrm{ADE}_{\mathrm{SM}}$, $\mathrm{BDE}_{\mathrm{SM}}$, ${}_{(\mathrm{FIGURE})}C_5$, and ${}_{(\mathrm{FIGURE})}C_6$. Wavefront testing of two field points is needed to solve all the parameters.

The computation model of misalignment and PM astigmatism figure error parameters of two-mirror telescopes is essentially a nonlinear system. In this paper, we use the medium-scale

fminunc algorithm in also MATLAB optimization toolbox to solve the misalignments.

3 Alignment Example

3.1 *Optical Design of R–C Telescope*

In this section, we will analyze and validate the correction effect of the model using an R–C telescope with astigmatism figure error on the PM. The simulation experiment includes three cases: simulation with and without wavefront testing error, and the Monte Carlo alignment simulations.

The optical design parameters of the R–C telescope are shown in Table 1. The aperture is 3 m, f number is 20, and the field of view is $2\omega = \pm 0.12$ deg.

The telescope is shown in Fig. 4, and the full-field display of Zernike coma (C_7 and C_8), Zernike astigmatism (C_5 and C_6), and RMS wavefront error are shown in Fig. 5. As can be seen from the Fig. 5, the R–C telescope is corrected for third-order coma, and the imaging field is limited by third-order astigmatism.

Table 1 Optical design parameters of the R–C telescope.

Surface	Type	Conic constant	Radius (mm)	Thickness (mm)
PM (stop)	Conic	−1.00212	−11214.953	−5000
SM	Conic	−1.48118	−1340.206	6499.984
Image	—	—	−625.954	—

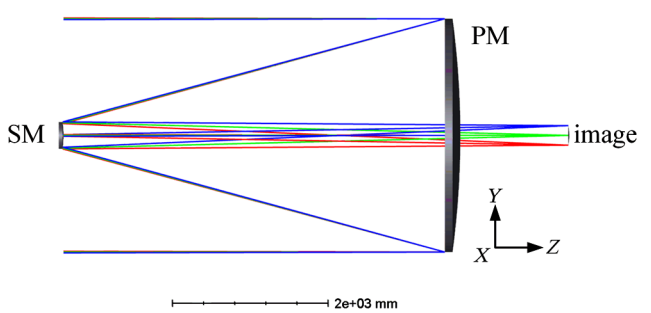

Fig. 4 The optical layout of the R–C telescope.

Table 2 Wavefront aberration coefficients of the R–C telescope.

Surface	W_{040} (λ)	W_{131} (λ)	W_{222} (λ)	W_{220M} (λ)	W_{311} (λ)
PM (spheric contributions)	1417.902	−88.812	1.391	0.695	0
PM (aspheric contributions)	−1420.911	0	0	0	0
SM (spheric contributions)	−166.495	45.119	−3.057	2.762	−0.581
SM (aspheric contributions)	169.504	43.693	2.816	2.816	0.181
sum	0	0	1.150	6.273	−0.400

Note: $\lambda = 632.8$ nm, similarly hereinafter.

The wavefront aberration coefficients of the telescope can be calculated by Code V, which are listed in Table 2.

3.2 *Case 1: Alignment Experiment without Wavefront Testing Error*

In this section, the computation model is used to calculate and correct the misaligned R–C telescope and the astigmatism error. The misalignments and figure errors of the telescope are introduced, as shown in Table 3.

The optical design software Code V is used to model the telescope. The full-field displays of Zernike astigmatism $C_{5/6}$ and Zernike coma $C_{7/8}$ are shown in Fig. 6.

As can be seen from Fig. 6, the binodal astigmatism and field-constant coma occur in the misaligned R–C system. We use wavefront testing results of two field points, a center field point ([0, 0]), and an external field point ([0.12 deg, 0]), to align this telescope.

Table 3 The misalignments and figure errors of the telescope.

XDE_{SM}	YDE_{SM}	ADE_{SM}	BDE_{SM}	$_{(FIGURE)}C_5$	$_{(FIGURE)}C_6$
−0.4 mm	0.3 mm	−0.04 deg	−0.08 deg	−0.11λ	0.09λ

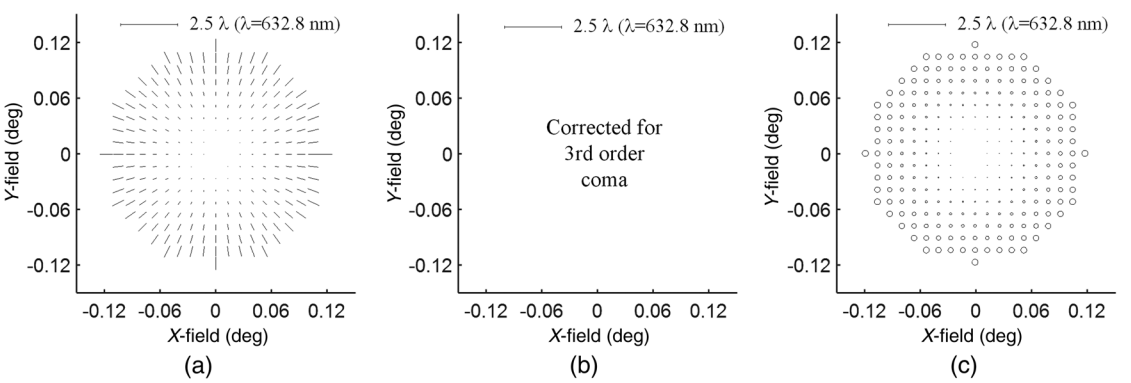

Fig. 5 FFDs for fringe Zernike coefficients (a) $C_{5/6}$, (b) $C_{7/8}$, and (c) RMS wavefront error for the nominal TMA telescope.

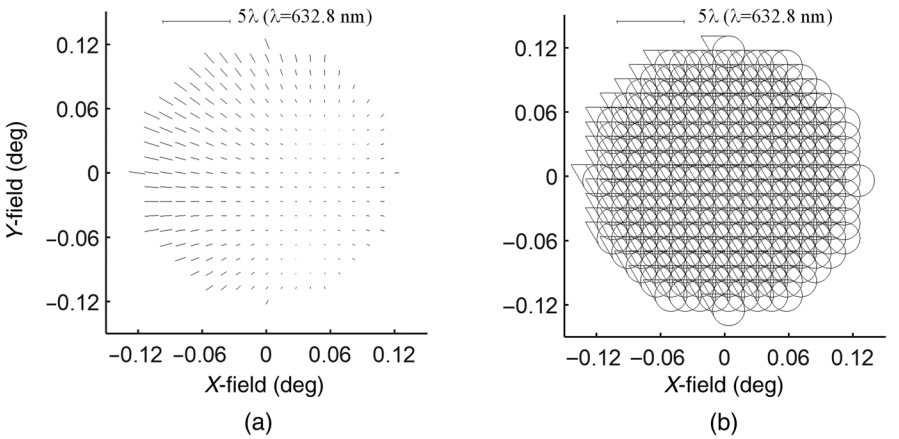

Fig. 6 Full-field displays of Zernike astigmatism and Zernike coma of misaligned telescope. (a) The Zernike astigmatism (C_5 and C_6) and (b) the Zernike coma (C_7 and C_8).

The steps of alignment simulation are as follows: first, we use the wavefront fitting function of Code V to obtain the Zernike coefficients of the wavefront of the two-field points, and then substitute the Zernike coefficients into the computation model so that we can get the quadratic equations about the misalignments and Zernike coefficients. The solution of the amount of misalignments can be obtained by solving the equation. Finally, the telescope is corrected with the misalignments and figure error of the solution, and the corrected optical system is compared with the nominal system and the initial misaligned system to verify the correction effect.

We use two iterative alignments to correct the misaligned telescope. The states of the optical system after each correction are shown in Fig. 7. In this paper, average and maximum RMS wavefront errors in the whole field of view are used to characterize the system's wave aberration state, which are calculated with $361(19 \times 19)$ equally spaced field points in a circular field whose angular radius is 0.12 deg.

The value of the residual misalignments and RMS wavefront error after each iteration alignment is shown in Table 4, and the values in the table are reserved for four digits after the decimal point.

It can be seen that the wavefront error basically reaches the nominal level after the first alignment, and the system changes is not obvious after the second correction. After the first alignment, the residual linear misalignments is about 10 μm, the residual angular misalignments is <1″, and the astigmatism figure error is fully corrected. It is shown that the computation model can accurately solve misalignments and figure error with the wavefront error data of two-field points.

Table 4 The optical system state after each iteration alignment.

	Nominal state	Original misaligned state	After the first alignment	After the second alignment
XDE_{SM} (mm)	—	−0.4	0.0103	0.0060
YDE_{SM} (mm)	—	0.3	−0.0030	0
ADE_{SM} (deg)	—	−0.04	0.0001	0
BDE_{SM} (deg)	—	−0.08	−0.0002	−0.0006
$_{(FIGURE)}C_5$ (λ)	—	−0.11	0	0
$_{(FIGURE)}C_6$ (λ)	—	0.09	−0.0001	0
Maximum RMS wavefront error (λ)	0.2665	1.6389	0.2673	0.2680
Average RMS wavefront error (λ)	0.1333	1.5591	0.1340	0.1333

3.3 *Case 2: Alignment Experiment with Wavefront Testing Error*

In the actual environment, there are some factors (airflow disturbance, vibration, etc.) that affect wavefront testing accuracy. These error sources can cause the Zernike coefficients obtained by wavefront testing to be inaccurate, and increase calculation

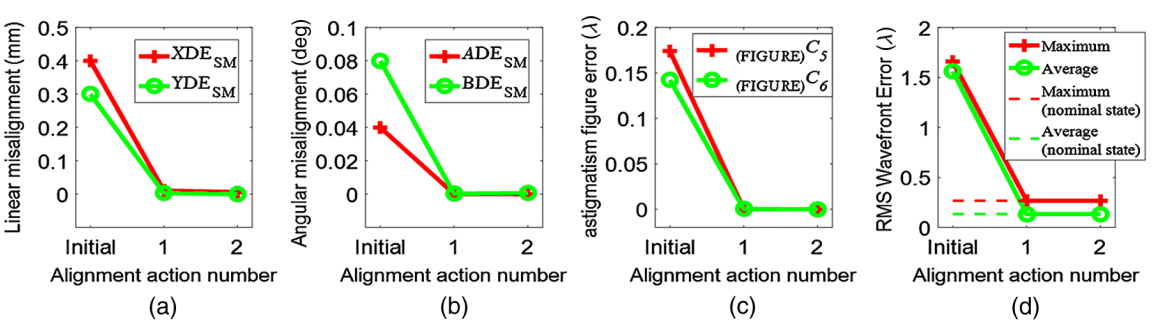

Fig. 7 The state of optical system after each correction. (a) Linear misalignment, (b) angular misalignment, (c) astigmatism figure error, and (d) RMS wavefront error.

error of the misalignments. So, it is necessary to analyze the influence of the wavefront testing error on computation model.

We will use the testing error model shown in Eq. (35) to simulate the correction effect of the model in the presence of wavefront testing error

$$C_{\mathrm{AST}} = \begin{bmatrix} C_5 - 3C_{12} \\ C_6 - 3C_{13} \end{bmatrix} + \begin{bmatrix} \varepsilon_{\mathrm{normrnd}(\mu=0,\sigma)} \\ \varepsilon_{\mathrm{normrnd}(\mu=0,\sigma)} \end{bmatrix}, \tag{35}$$

$$C_{\mathrm{COMA}} = \begin{bmatrix} C_7 - C_{10} - 4C_{14} \\ C_8 - C_{11} - 4C_{15} \end{bmatrix} + \begin{bmatrix} \varepsilon_{\mathrm{normrnd}(\mu=0,\sigma)} \\ \varepsilon_{\mathrm{normrnd}(\mu=0,\sigma)} \end{bmatrix}. \tag{36}$$

An error amount $\varepsilon_{\mathrm{normrnd}(\mu,\sigma)}$ is added to C_{AST} and C_{COMA}. $\varepsilon_{\mathrm{normrnd}(\mu,\sigma)}$ is a random value that follows a normal distribution (the mean is μ, the standard deviation is σ), and it is used to simulate random testing error. To compare with the experimental results without wavefront testing error, we still use the misalignment system shown in Table 3 to perform a large number of misalignments correction experiments with random error effects. We use four different combinations of field points to calculate the misalignments to further verify the effect of the number of field points on the correction effect of the optical system. The four combinations of field points are shown in Table 5 and Fig. 8.

Table 5 Four combinations of field points.

Combination 1	Combination 2	Combination 3	Combination 4
①②	①②⑥	①②④⑥⑧	①②③④⑤⑥⑦⑧⑨

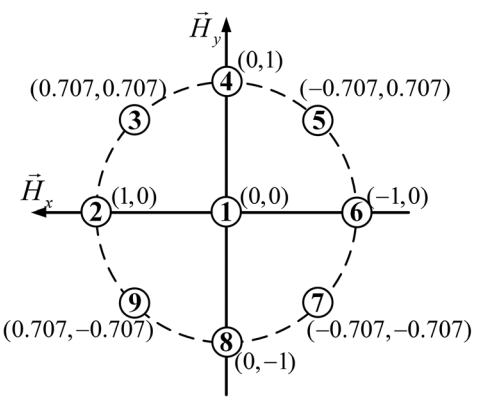

Fig. 8 Field points used in wavefront testing.

The wavefront testing errors are divided into three levels according to the magnitude in the error experiment, whose σ are 0.1, 0.175, and 0.25 λ, respectively. The computation model is used to correct the misaligned system twice, and the correction results obtained with four different field combinations are shown in Fig. 9. The different color curves represent different testing error levels.

It can be seen from Fig. 9 that the robustness of the computation model is good. For example, when $\sigma = 0.25\,\lambda$ and the number of field points for testing is 5, the standard deviation of the average RMS wavefront error in the field of view is only 0.019 λ, and the standard deviation of the maximum RMS wavefront error in the field of view is only 0.00821 λ.

It can also be seen that, in the presence of testing error, if only two-field points are used for wavefront testing, the correction results are poor. And an increase in the number of field points for testing is able to effectively enhance the robustness of the computation model. Taking the results of the average RMS wavefront error as an example, the standard deviation of the three different σ values decreased by 74.3% ($\sigma = 0.1\,\lambda$), 77.6% ($\sigma = 0.175\,\lambda$), and 70% ($\sigma = 0.25\,\lambda$), respectively, when the field points for testing increase from 2 to 5. It can also be seen that the standard deviations in the three cases decreased by 26.8% ($\sigma = 0.1\,\lambda$), 20.8% ($\sigma = 0.175\,\lambda$), and 27.5% ($\sigma = 0.25\,\lambda$), respectively, when the field points for testing increase from 5 to 9. Therefore, when the field points for testing is more than 5, increasing the field points for testing to suppress testing error will not receive significant results. Meanwhile, increasing the field points results in an increase in testing time, which is also disadvantageous for improving the correction frequency.

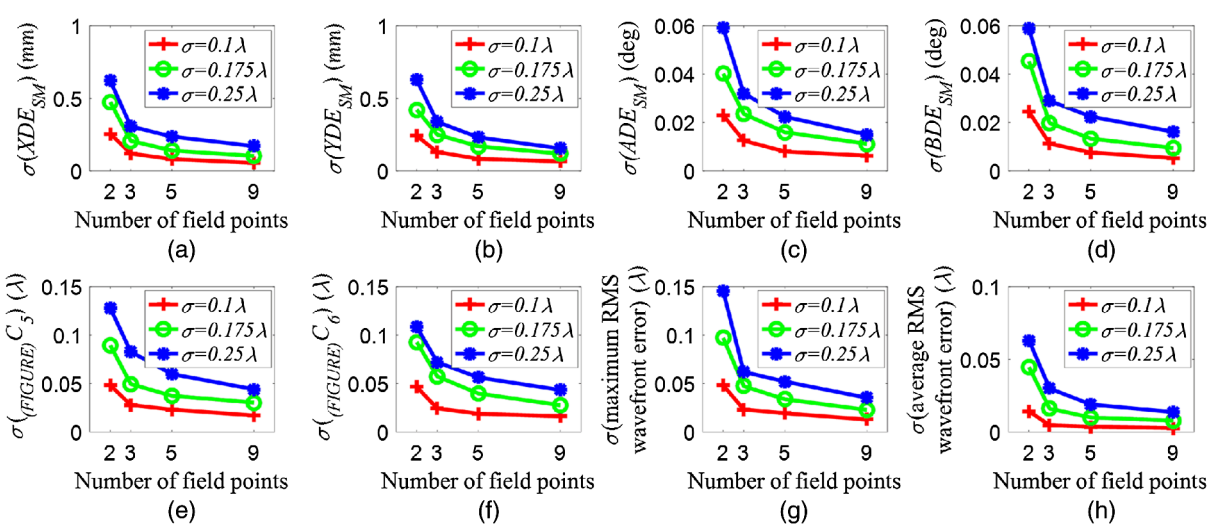

Fig. 9 The relationship between the standard deviation of (a) XDE, (b) YDE, (c) ADE, (d) BDE, (e) $_{(\mathrm{FIGURE})}C_5$, (f) $_{(\mathrm{FIGURE})}C_6$, (g) maximum RMS wavefront error, and (h) average RMS wavefront error of 100 trials and the number of field points used for wavefront testing and the error levels.

The intervals of the three curves of different testing error levels are roughly equal, so the error is basically linearly related to the standard deviation of the parameters (misalignments, figure error, and wavefront error) after correction.

3.4 *Case3: Monte Carlo Alignment Simulations*

The amount of misalignments is random values in actual alignment, and their size is closely related to the accuracy of the coarse alignment. In Secs. 3.2 and 3.3, we discuss the effect of correcting the model in a particular misaligned state, ignoring the randomness of the value of misalignments, and the effect of the magnitude of the misalignments on the effect of the correction is not analyzed.

In this section, the Monte Carlo alignment simulations are carried out to discuss the correction effect in different misalignment ranges and different error values, and verify the corrective ability more generally and objectively.

There are three different misalignment ranges for simulations as shown in Table 6.

The experimental process is as follows: we generate 100 pairs of pseudorandom misalignment values following a standard uniform distribution for each range. Each of these misaligned states is introduced in the simulation software Code V and the wavefront errors can be obtained. As a result, we have 300 pairs of misalignments for all ranges, which represent 300 misaligned systems. Each of the misaligned systems performs misalignment correction at four different wavefront testing error levels, which are $\sigma = 0$, $\sigma = 0.1\,\lambda$, $\sigma = 0.175\,\lambda$, and $\sigma = 0.25\,\lambda$. Misalignment correction is performed using the five field points in combination three as shown in Table 5. Figure 10 shows the results of two iterative corrections of each misaligned system at different error levels. $(\mathrm{WFE}_{\mathrm{rms}}^{\mathrm{MAX}})_i^{\mathrm{corrected}}$ and $(\mathrm{WFE}_{\mathrm{rms}}^{\mathrm{AVE}})_i^{\mathrm{corrected}}$ are the maximum and average RMS wavefront errors in the field of view of the i'th trial after misalignment correction, respectively, $(\mathrm{WFE}_{\mathrm{rms}}^{\mathrm{MAX}})^{\mathrm{nominal}}$ and $(\mathrm{WFE}_{\mathrm{rms}}^{\mathrm{AVE}})^{\mathrm{nominal}}$ are the maximum and average RMS wavefront errors in the field of view of the i'th trial in the nominal state, respectively, which are given in Table 4. $(\mathrm{WFE}_{\mathrm{rms}}^{\mathrm{MAX}})^{\mathrm{nominal}} = 0.2665\,\lambda$, $(\mathrm{WFE}_{\mathrm{rms}}^{\mathrm{AVE}})^{\mathrm{nominal}} = 0.1333\,\lambda$.

Table 6 The range of random misalignments.

	XDE and YDE (mm)	ADE and BDE (deg)	$_{(\mathrm{FIGURE})}C_{5/6}$ (λ)
Range 1	[−0.5, 0.5]	[−0.02, −0.02]	[−0.05, 0.05]
Range 2	[−1,1]	[−0.05, 0.05]	[−0.1, 0.1]
Range 3	[−2,2]	[−0.1, 0.1]	[0.2, −0.2]

Figure 10 shows the relationship between the root mean square deviation (RMSD) of the maximum/average RMS wavefront error and the error levels. The RMSD is defined as

$$\mathrm{RMSD} = \sqrt{\frac{1}{n}\sum_{i=1}^{n}\left[(\mathrm{WFE}_{\mathrm{rms}}^{\mathrm{MAX/AVE}})_{\mathrm{i}}^{\mathrm{corrected}} - (\mathrm{WFE}_{\mathrm{rms}}^{\mathrm{MAX/AVE}})^{\mathrm{nominal}}\right]^2}, \tag{37}$$

where n is the number of trials, and $n = 100$; i is the trial number.

According to the Monte Carlo simulation analysis results, it can be seen that, in the absence of wavefront testing error, the correction effects of all of the trials do not deteriorate as the amount of misalignment increased. After two iterative corrections, the RMSD of the average RMS wavefront error of the 300 trials is on the order of $10^{-6}\,\lambda$, and the RMSD of the maximum RMS wavefront error is on the order of $10^{-5}\,\lambda$. It can be considered that all of the misaligned systems after the correction have reached the nominal state.

In the presence of wavefront testing error, the magnitude of the error is closely related to the results of correction. The RMSD of wavefront error increases with an increase in the error, and it is roughly linear. The effect of wavefront testing error on the RMSD of the maximum RMS wavefront error is more significant than the average RMS wavefront error. It can also be seen that the magnitude of the error is the main factor that affects the correction results, while the magnitude of the misalignments has little effect, which shows that the model also has good correction capability for systems with large misalignments.

4 Conclusion

This paper mainly studies the computation method based on the NAT of misalignments and PM astigmatism figure error parameters of two-mirror telescopes. We deduces the expressions of the aberration field decenter vectors and analyzes third-order astigmatism and coma aberration field for a misaligned two-mirror telescope with astigmatism figure error on PM. In addition,

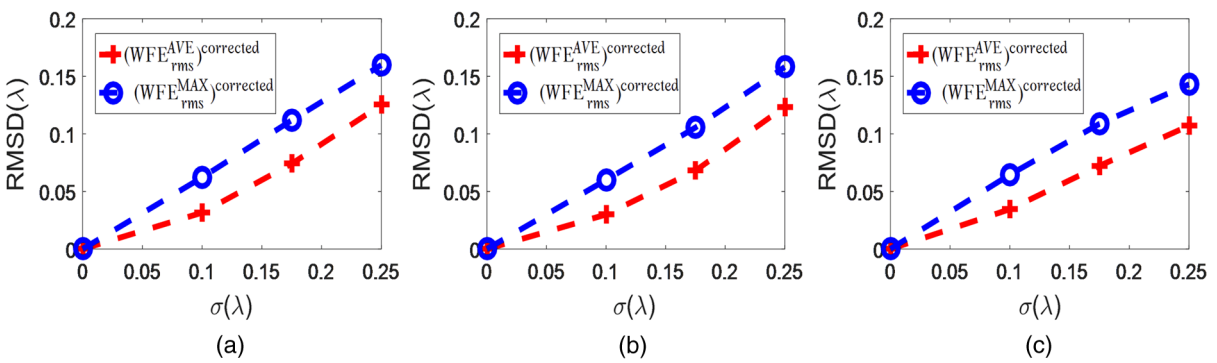

Fig. 10 The relationship between the RMSD of the maximum/average RMS wavefront error and the error levels for (a) range 1, (b) range 2, and (c) range 3 of random misalignments.

an R–C telescope is used to carry out alignment simulations with the computational model.

The simulation experiment without wavefront testing error shows that the misaligned system can be corrected to be close to the nominal state after the 1st alignment with wavefront testing of two-field points.

The simulation experiment with wavefront testing error shows that an increase in the number of field points for wavefront testing can effectively improve the robustness of the computation model, but when the number of field points for wavefront testing is more than 5, significant results will not be received by simply increasing the field points to suppress testing error. It also can be found that the wavefront testing error is essentially linear with the standard deviation of misalignments, figure error, and RMS wavefront error after correction.

Monte Carlo simulation results show that, in the absence of wavefront testing error, the correction effect of all the trials does not deteriorate with an increase in the amount of misalignments. In the presence of wavefront testing error, the RMSD of the wavefront error after the correction of the trials increases as the wavefront testing error increases and they are roughly linear. The wavefront testing error is the main factor that affects the RMSD of the wavefront error after correction, while the magnitude of the misalignments has little effect on it.

Acknowledgments

This work was supported by the National Key Research and Development Program (2016YFF0103603).

References

1. B. A. McLeod, "Collimation of fast wide-field telescopes," *Publ. Astron. Soc. Pac.* **108**(720), 217 (1996).
2. L. Noethe and S. Guisard, "Analytical expressions for field astigmatism in decentered two mirror telescopes and application to the collimation of the ESO VLT," *Astron. Astrophys. Suppl. Ser.* **144**(1), 157–167 (2000).
3. R. Holzlöhner et al., "Fast active optics control of wide-field telescopes based on science image analysis," *Proc. SPIE* **9151**, 91512I (2014).
4. J. Sasián et al., "Active reconstruction and alignment strategies for the advanced technology solar telescope," *Proc. SPIE* **7793**, 77930E (2010).
5. L. M. Stepp et al., "Active optics in large synoptic survey telescope," *Proc. SPIE* **8444**, 84444Q (2012).
6. H. Lee et al., "Computer-guided alignment I: phase and amplitude modulation of alignment-influenced optical wavefront," *Opt. Express* **15**(6), 3127–3139 (2007).
7. H. Lee et al., "Computer-guided alignment II: optical system alignment using differential wavefront sampling," *Opt. Express* **15**(23), 15424–15437 (2007).
8. S. Kim et al., "Merit function regression method for efficient alignment control of two-mirror optical systems," *Opt. Express* **15**(8), 5059–5068 (2007).
9. R. B. Johnson et al., "Method for determining individual element misalignments in optical systems," *Proc. SPIE* **8486**, 848617 (2012).
10. J. M. Sasian et al., "Misalignment parameters estimation in refractive optical systems," *Proc. SPIE* **7068**, 70680P (2008).
11. K. P. Thompson and J. P. Rolland, "A page from 'the drawer': how Roland Shack opened the door to the aberration theory of freeform optics," *Proc. SPIE* **9186**, 91860A (2014).
12. R. V. Shack and K. P. Thompson, "Influence of alignment errors of a telescope system on its aberration field," *Proc. SPIE* **0251**, 146–153 (1980).
13. K. P. Thompson, "Description of the third-order optical aberrations of near-circular pupil optical systems without symmetry," *J. Opt. Soc. Am. A* **22**(7), 1389–1401 (2005).
14. K. P. Thompson, "Aberration fields in tilted and decentered optical systems," PhD Dissertation, University of Arizona, Arizona (1980).
15. K. P. Thompson et al., "Real-ray-based method for locating individual surface aberration field centers in imaging optical systems without rotational symmetry," *J. Opt. Soc. Am. A* **26**(6), 1503–1517 (2009).
16. K. P. Thompson, "Multinodal fifth-order optical aberrations of optical systems without rotational symmetry: spherical aberration," *J. Opt. Soc. Am. A* **26**(5), 1090–1100 (2009).
17. K. P. Thompson, "Multinodal fifth-order optical aberrations of optical systems without rotational symmetry: the comatic aberrations," *J. Opt. Soc. Am. A* **27**(6), 1490–1504 (2010).
18. K. P. Thompson, "Multinodal fifth-order optical aberrations of optical systems without rotational symmetry: the astigmatic aberrations," *J. Opt. Soc. Am. A* **28**(5), 821–836 (2011).
19. T. Schmid, K. P. Thompson, and J. P. Rolland, "A unique astigmatic nodal property in misaligned Ritchey–Chrétien telescopes with misalignment coma removed," *Opt. Express* **18**(5), 5282–5288 (2010).
20. T. Schmid et al., "Separation of the effects of astigmatic figure error from misalignments using nodal aberration theory (NAT)," *Opt. Express* **18**(16), 17433–17447 (2010).
21. R. A. Buchroeder, "Tilted component optical systems," PhD Dissertation, University of Arizona, Arizona (1976).
22. R. K. Tyson, "Conversion of Zernike aberration coefficients to Seidel and higher-order power-series aberration coefficients," *Opt. Lett.* **7**(6), 262–264 (1982).

Zhiyuan Gu is a research assistant at Changchun Institute of Optics, Fine Mechanics and Physics, Chinese Academy of Science. He received his BS and PhD degrees in optical engineering from Dalian University of Technology in 2009 and from the University of Chinese Academy of Sciences in 2016, respectively. His research interests include active optical correction algorithms for large aperture telescope, optical system alignment, and unconventional optical system design.

Yang Wang is a lecturer at Changchun University of Science and Technology. She received her BS degree from Changchun University of Science and Technology in 2009 and her PhD from the University of Chinese Academy of Sciences in 2014. Her research interests are optomechanical design and optical system design. Her teaching interests mainly include fundamentals of optical design and optical measurements.

Guohao Ju is a research assistant at Changchun Institute of Optics, Fine Mechanics and Physics, Chinese Academy of Science, majoring in active optics.

Changxiang Yan is a professor at the Changchun Institute of Optics, Fine Mechanics and Physics, Chinese Academy of Science. His research interests include space optical remote sensing technology, multispectral, and hyperspectral remote sensing imaging technology.